Adv. Composite Mater., Vol. 16, No. 2, pp. 181–194 (2007)

Also available online - www.brill.nl/acm

Mechanical properties of ABS resin reinforced with recycled CFRP

KEIJI OGI [1,*], TAKASHI NISHIKAWA [2], YASUTAKA OKANO [2] and ICHIRO TAKETA [2]

[1] *Graduate School of Science and Engineering, Ehime University, 3 Bunkyocho, Matsuyama, Ehime 790-8577, Japan*
[2] *Toray Industries, Inc., 1515, Tsutsui, Masaki-cho, Ehime 791-3193, Japan*

Received 3 October 2005; accepted 17 August 2006

Abstract—This paper presents the mechanical properties of a composite consisting of acrylonitrile-butadiene-styrene (ABS) resin mixed with carbon fiber reinforced plastics (CFRP) pieces (CFRP/ABS). CFRP pieces made by crushing CFRP wastes were utilized in this material. Nine kinds of CFRP/ABS compounds with different weight fraction and size of CFRP pieces were prepared. Firstly, tensile and flexural tests were performed for the specimens with various CFRP content. Next, fracture surfaces of the specimens were microscopically observed to investigate fracture behavior and fiber/resin interface. Finally, the tensile modulus and strength were discussed based on the macromechanical model. It is found that the elastic modulus increases linearly with increasing CFRP content while the strength changes nonlinearly. Microscopic observation revealed that most carbon fibers are separated individually and dispersed homogeneously in ABS resin. Epoxy resin particles originally from CFRP are dispersed in ABS resin and seem to be in good contact with surrounding resin. The modulus and strength can be expressed using a macromechanical model taking account of fiber orientation, length and interfacial bonding in short fiber composites.

Keywords: CFRP; thermoplastic resin; recycle; mechanical properties; interface.

1. INTRODUCTION

Since carbon fiber reinforced plastics (CFRP) have excellent mechanical properties, such as high specific strength and modulus, they have been used as light-weight structural materials for aerospace vehicles, automobiles, and so on. As the demand for CFRP increases, the technique of recycling CFRP wastes should be established in the near future.

Edited by the JSCM.

*To whom correspondence should be addressed. E-mail: kogi@eng.ehime-u.ac.jp

In general, recycling of CFRP is thought to be difficult because of its hardness and chemical stability. Recycling methods are classified into material recycling, chemical recycling and thermal recycling. In material recycling, wasted CFRPs are directly utilized through mixture with base material. A project to establish the recycling system of glass fiber reinforced plastics (GFRPs) was conducted by Government Industrial Research Institutes (GIRIS, former AIST) in Japan [1]. As part of the material recycling in this project, a device to cut large scale GFRP wastes from equipment such as boats was developed and also some composites including crushed GFRP were fabricated. More recently, an attempt has been made to develop new concrete reinforced with crushed CFRP pieces [2] in a project for establishing crushing and classification technique of CFRP wastes in Japan. However, most of CFRP wastes are presumed to be buried in the ground or left as they are, and it is estimated that five thousand tons of CFRP are wasted in a year world-wide. As far as the authors know, few commercial products using recycled CFRP have been reported although some research may be conducted in laboratories. Consequently, a recycling system for CFRP wastes has not been established anywhere so far.

The authors have recently developed an electromagnetic shield material using recycled CFRP pieces as conductive fillers and its electrical properties including shield effect have been evaluated [3]. Since carbon fibers are used in this material, it is expected that mechanical properties are also improved. Much work has been conducted on the mechanical behavior of short fiber composites made of virgin and recycled fibers [4–15]. Macro- and micromechanical models in the previous study have employed the shear lag models to express the modulus and strength of short fiber composites. Thomason [14, 15] has discussed the effect of fiber length distribution on the mechanical properties in short glass-fiber reinforced composites. Eriksson *et al.* [6] has reported the mechanical properties of recycled glass-fiber reinforced polyamide resin and predicted the strength based on the Kelly–Tyson model [5].

In this paper, nine kinds of compounds with different weight fraction and size of CFRP pieces were prepared for the measurement of mechanical properties. Firstly, tensile and flexural tests were performed to investigate the effect of CFRP content on the strength and elastic modulus. Next, the fracture surfaces of the specimens were microscopically observed to investigate fracture behavior and the interface between fiber and resin. Finally, elastic modulus and strength were discussed based on a macromechanical model taking into account the effect of fiber orientation and length and interfacial shear stress.

2. EXPERIMENTAL PROCEDURE

2.1. Material

The used wastes are epoxy resin reinforced with carbon fiber (T700S, Toray) and the fiber volume fraction is 0.60. Figure 1 shows a schematic of the machine used

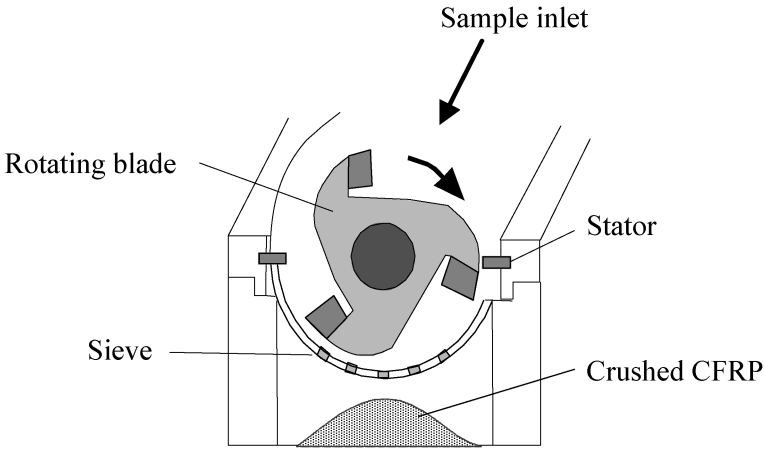

Figure 1. A schematic of a crushing machine for recycling CFRP wastes.

for crushing CFRP wastes into pieces. The CFRP pieces with the average length by width of 3.4×0.4 mm^2 were employed. The variation in length was 1 to 10 mm. Some CFRP pieces experienced a further crushing by a ball mill to investigate the effect of CFRP size on mechanical properties. Most of the milled CFRP pieces were in the state of particles with the size of 1 to 10 μm. Crushed CFRP pieces made of carbon fibers and epoxy resin include a lot of individually separated fibers and some fiber bundles of large size. Figure 2 shows SEM photos showing separated carbon fibers and a fiber bundle. Most part of the surface of separated carbon fibers is not already coated by epoxy resin although fiber bundles originating from CFRP contain epoxy resin.

The specimens consisting of acrylonitrile-butadiene-styrene (ABS) resin and CFRP pieces were fabricated through mixing, grinding and injection molding procedures. Eight kinds of composite specimens with different weight fraction and size of CFRP pieces in addition to ABS resin specimens were prepared for measuring mechanical properties. Table 1 summarizes mixture ratio of the specimens. The weight fraction of CFRP pieces varies from 0 to 0.7 for the specimens Nos 1 to 8. The milled CFRP pieces were used in No. 9 specimens. Fiber volume fraction V_f of the composite is calculated through V_f (=0.6) of CFRP and density of CFRP and ABS resin.

Figure 3 shows optical micrographs showing the polished surface of specimen No. 6. Most carbon fibers are separated individually and dispersed homogeneously in ABS resin whilst a few fiber bundles are observed. This implies that the mechanical properties of CFRP pieces before fabrication make little contribution to those of the compounds. Fibers and fiber bundles near the surface are oriented along the direction of injection flow denoted by the arrows; on the other hand, fibers inside the specimen are randomly oriented as shown in the fracture surface. The length of fibers observed on the polished surface was measured. The measured fiber

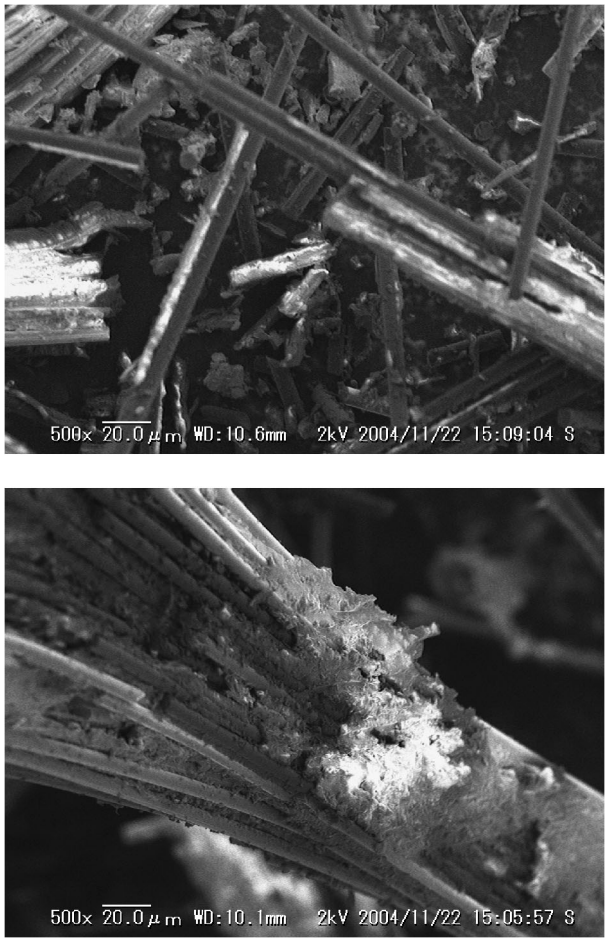

Figure 2. SEM photos of CFRP pieces; top: separated fibers, bottom: fiber bundle.

Table 1.
Mixture ratio of CFRP/ABS composites

No	CFRP	ABS	V_f
1	0.0	1.0	0.000
2	0.1	0.9	0.041
3	0.2	0.8	0.085
4	0.3	0.7	0.132
5	0.4	0.6	0.182
6	0.5	0.5	0.238
7	0.6	0.4	0.298
8	0.7	0.3	0.364
9	0.3*	0.7	0.132

* Milled CFRP pieces.

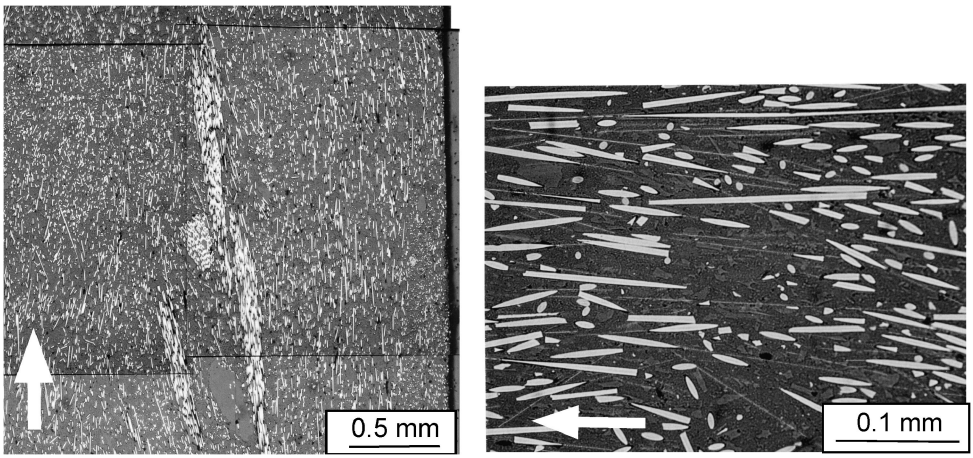

Figure 3. Optical micrographs of polished surface of a No. 6 specimen.

length varies from 100 to 250 μm and the average is 200 μm. The bending and winding of fibers are not considered here.

2.2. Mechanical tests

At first, tensile tests were performed using an electrohydraulic testing machine for dumbbell-type specimens (JIS K7139, gage length 100 mm, width 10 mm, thickness 4 mm). A strain gage was adhesively bonded on the specimen surface to measure the elongation and calculate the Young's modulus. Next, flexural tests were conducted using the same testing machine for coupon specimens (80 mm × 10 mm × 4 mm) cut from the dumbbell-type specimens. Flexural strength and modulus were calculated from the load–displacement curve. Both mechanical tests were carried out at a room temperature. Five specimens were employed for each kind of compounds in each mechanical test.

2.3. Microscopic observation

Fracture surface was observed using scanning electron microscopy (SEM) to characterize the fracture behavior focusing on the interface between fiber and resin. Elements which appeared on the fracture surface were identified and their weight fractions were calculated using an electron probe micro analyzer (EPMA).

3. RESULTS AND DISCUSSION

3.1. Mechanical properties

Figure 4 shows typical tensile stress–strain curves for all the specimens. The stress–strain behavior of all the specimens is nonlinear after the first linear portion at low

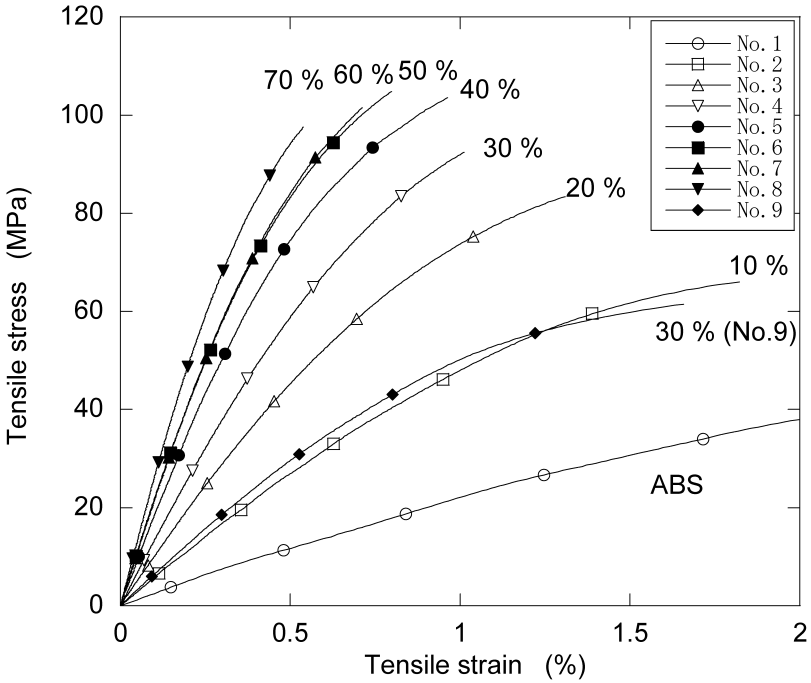

Figure 4. Typical tensile stress–strain curves for the specimens.

strains. The stress–strain curve at linear elastic portion can be described using the modified rule of mixture as discussed in Section 3.3. Nonlinearity is considered to be attributed to microscopic damage, such as interfacial debonding and resin cracking [16]. Figure 5 shows tensile and flexural strength against CFRP content. Both strength increases with increasing CFRP content below 50 wt%. After the strength reaches the maximum at around 50 wt%, it decreases slightly at higher CFRP content. Figure 6 shows tensile and flexural modulus against CFRP content. Both moduli increase almost linearly with CFRP content and obey the rule of mixture, as discussed later. Very similar behavior on strength and modulus of short fiber composites has been reported by Thomason [14, 15]. The strength and modulus of a No. 9 specimen having milled CFRP pieces are much lower than those of No. 4 specimen with the same CFRP content. One of the reasons for this low strength and modulus of a No. 9 specimen is the low efficiency of reinforcement due to fiber length (<10 μm) shorter than the critical one as discussed in Section 3.3. Figure 7 depicts failure strain in the tensile tests as a function of CFRP content. The failure strain decreases with an increase in CFRP content and its rate of decrease is constant. It is supposed that the strength is approximately expressed as a product of elastic modulus and failure strain. The modulus increases while the failure strain decreases approximately linearly with CFRP content. As a result, strength becomes the maximum at around 50 wt%.

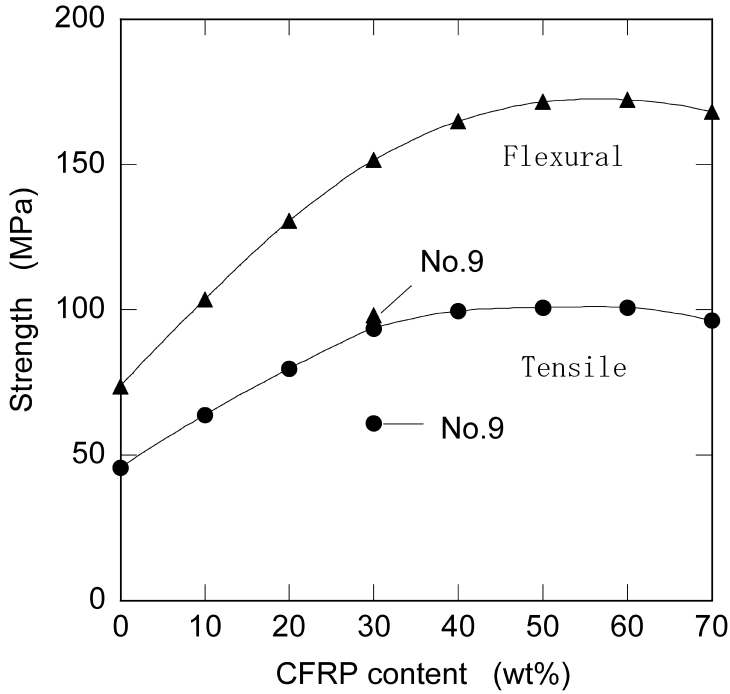

Figure 5. Tensile and flexural strength as a function of CFRP content.

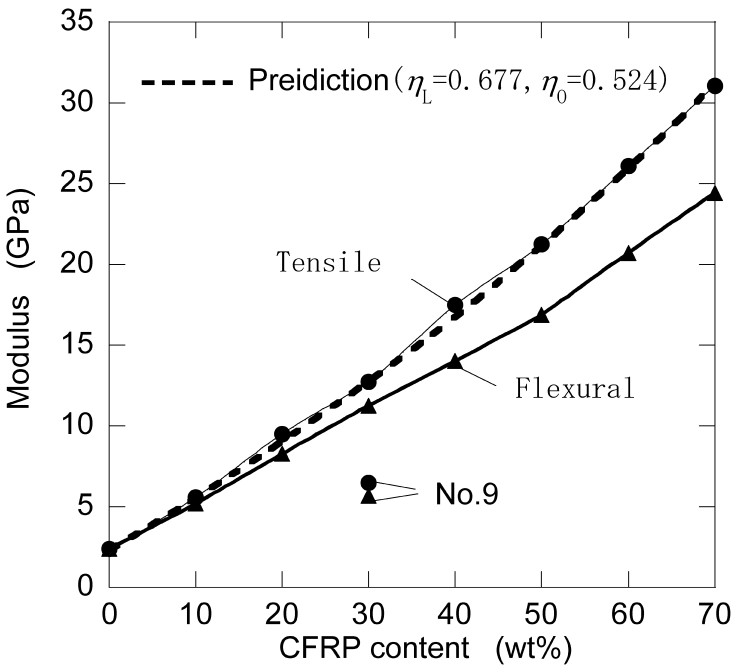

Figure 6. Tensile and flexural modulus as a function of CFRP content.

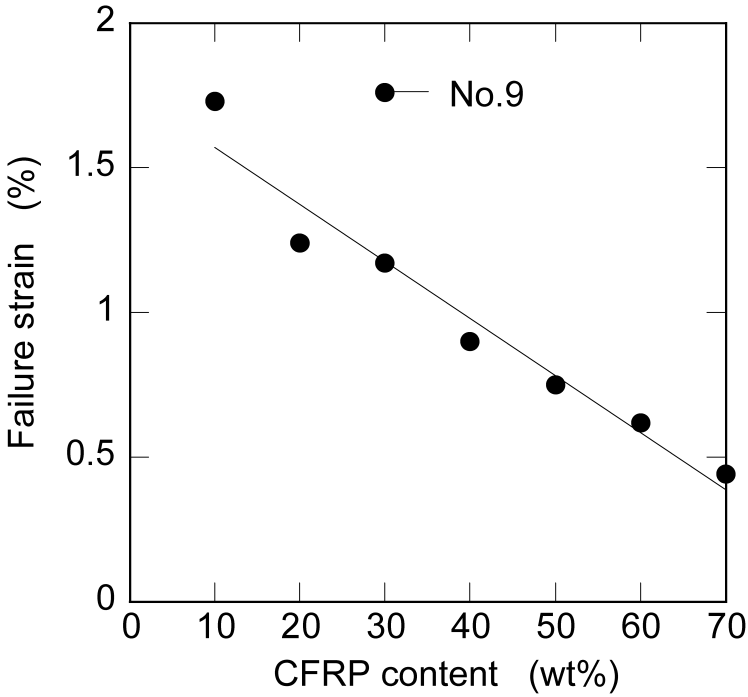

Figure 7. Failure strain in the tensile tests as a function of CFRP content.

3.2. Fractography

Figure 8 shows a SEM photograph showing the fracture surface after the tensile test of specimen No. 6 (50 wt%). Some fibers are pulled out from the resin and randomly oriented rather than in the flow direction perpendicular to the fracture surface. Figure 9 shows elements mapping image corresponding to Fig. 8. The resin observed on the surface of a carbon fiber, indicated by arrow A, is identified as ABS resin because oxygen is poor in this area. On the other hand, the particle indicated by arrow B is identified as epoxy resin which contains relatively rich oxygen. Hence it is presumed that epoxy resin surrounding carbon fiber is removed from the fiber during crushing and fabrication processes and that carbon fiber is not coated by epoxy resin. This fact is important for conductive materials because conductive paths can be formed when fibers are in contact with each other or appropriate conductive filler is added.

3.3. Macromechanical model

In this section, tensile elastic modulus and strength are discussed based on a macromechanical model. In general, injection-molded specimens have heterogeneity in fiber orientation. As shown in Figs 3 and 8, fibers near the surface are oriented along the direction of injection flow while fibers inside the specimen are randomly

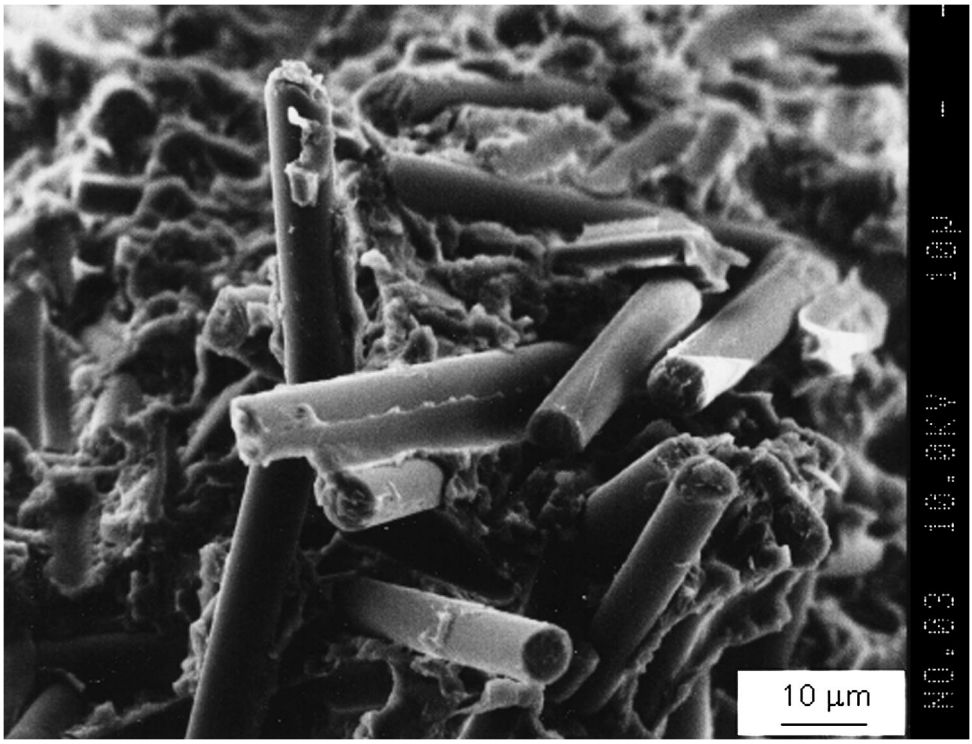

Figure 8. A SEM photo showing fracture surface of a No. 6 specimen after a tensile test.

oriented. Hence, hereafter, macroscopic mechanical properties are discussed under the assumption that fibers are homogeneously oriented in the overall specimen.

Elastic modulus of short fiber composites, denoted by E_C, can be predicted by the following modified rule of mixture [16]:

$$E_C = \eta_O \eta_L E_f V_f + E_m(1 - V_f), \tag{1}$$

where E_f and E_m denote elastic modulus of fiber and matrix, respectively; η_O and η_L represent factors with respect to fiber orientation and fiber length, respectively; and V_f is fiber volume fraction. The orientation factor η_O is 0.375 for perfectly in-plane random distribution and 0.20 for three-dimensional random distribution [16], however, it is larger for injection-molded short fiber composites due to effect of flow [14]. The length factor is expressed by [4]

$$\eta_L = 1 - \frac{\tanh(\beta \bar{l}/2)}{\beta \bar{l}/2} \tag{2}$$

with

$$\beta = \left(\frac{2G_m}{E_f r^2 \ln(1/\sqrt{V_f})} \right)^{1/2}, \tag{3}$$

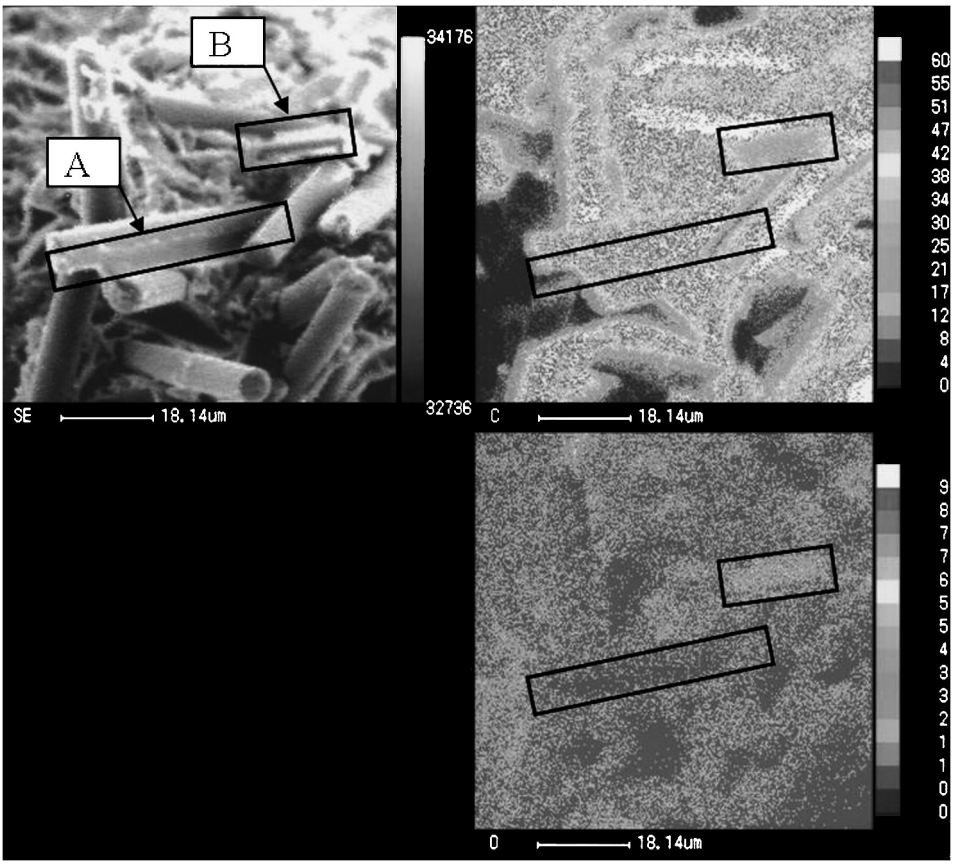

Figure 9. EPMA mapping images corresponding to Fig. 8 (upper left: SEM, upper right: carbon, lower right: oxygen).

where $\bar{l}$ and r denote the average length and radius of fiber, respectively, and G_{m} denotes the shear modulus of resin. Because the true value of the orientation factor is unknown for the present composite, it needs to be estimated for given material parameters. From $E_{\mathrm{f}} = 230$ GPa, $E_{\mathrm{m}} = 2.3$ GPa, $r = 3.5$ μm, $\bar{l} = 200$ μm and $V_{\mathrm{f}} = 0.3$ with the aid of equations (2) and (3), the length factor η_{L} is calculated to be 0.677. Since $\eta_{\mathrm{O}}\eta_{\mathrm{L}} = 0.355$ gives the best agreement with the experimental results regarding tensile elastic modulus (see the dotted line in Fig. 6), the orientation factor η_{O} is calculated to be 0.524. This value is larger than those for in-plane or three-dimensional random distributions. This result means that the ratio of fibers oriented in the injection (length) direction is higher than in the case of the random distributions. In addition, since η_{L} is smaller than unity, the present specimens are sure to be regarded as short fiber composites.

Next, the composite stress σ_C at given strain ε_C is given by [6, 14]

$$\sigma_C = \eta_O\left(\sum_{l_i=0}^{l_i=l_C}\frac{\tau l_i V_i}{2r} + \sum_{l_j=l_C}^{l_j=\infty}\left[E_f\varepsilon_C V_j\left(1-\frac{E_f\varepsilon_C r}{2\tau l_j}\right)\right]\right) + (1-V_f)\sigma_m(\varepsilon_C), \quad (4)$$

where τ and σ_m are the average fiber/resin interfacial shear stress and stress in the resin, respectively, V_i denotes volume fraction of fiber with the length l_i and l_C represents the critical fiber length given by

$$l_C = \frac{\sigma_f^* r}{\tau^*}, \quad (5)$$

where σ_f^* and τ^* denote the fiber and interfacial strength. The length l_C is estimated to be 340 μm using $\sigma_f^* = 4800$ MPa and $\tau^* = 50$ MPa which are typical values for CFRP composites. Because most of the fibers have the length shorter than the critical one, equation (4) is rewritten as

$$\sigma_C = \eta_O\frac{\tau\bar{l}V_f}{2r} + (1-V_f)\sigma_m(\varepsilon_C). \quad (6)$$

Thus, the composite strength is given by

$$\sigma_C^* = \eta_O\frac{\tau_u\bar{l}V_f}{2r} + (1-V_f)\sigma_m(\varepsilon_C^*), \quad (7)$$

where σ_C^* and ε_C^* represent the strength and failure strain of the composite, τ_u denotes the applied average interfacial shear stress at failure and $\sigma_m(\varepsilon_C^*)$ is the stress in the resin at $\varepsilon_C = \varepsilon_C^*$ calculated using the stress–strain curve of ABS resin in Fig. 4. Unlike the previous work, τ_u does not always mean the constant interfacial shear strength, but it depends on fiber volume fraction. Table 2 summarizes the measured composite strength, failure strain, applied resin stress and applied interfacial shear stress at failure calculated using equation (7). Figure 10 illustrates the strength of composite (σ_C^*), applied stress in the resin (σ_m) and applied shear stress at the interface (τ_u) at failure as well as contributions of the first and second terms to σ_C^* in equation (7). The resin stress σ_m decreases with fiber volume fraction

Table 2.
Failure stress and strain of composites and the applied stress in the resin and at the interface

Specimen No.	V_f	ε_C^*	σ_C^* (MPa)	$\sigma_m(\varepsilon_C^*)$ (MPa)	τ_u (MPa)
2	0.041	0.0173	63.9	34.2	50.7
3	0.085	0.0124	79.8	26.6	43.6
4	0.132	0.0117	93.6	25.4	36.2
5	0.182	0.009	99.6	20.1	30.5
6	0.238	0.0075	100.8	16.7	24.7
7	0.298	0.0062	100.8	14.1	20.4
8	0.364	0.0044	96.35	10.4	16.5

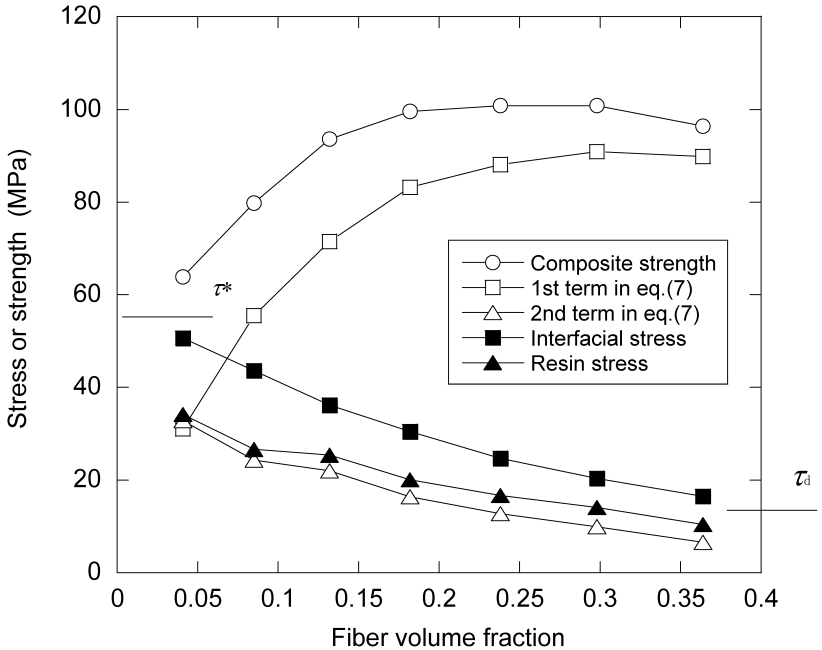

Figure 10. Strength of the composite and applied stress in the resin and at the interface at failure.

V_f since the failure strain decreases with V_f. Hence, the second term decreases and the first term increases with V_f. Nevertheless, the interfacial shear stress τ_u decreases with V_f. Figure 11 indicates the stress and strain at which the tensile stress–strain curve deviates from a linear relation. The knee point strain gradually decreases with V_f while the knee point stress increases for less than $V_f = 0.18$ and becomes almost constant (34 to 35 MPa) for V_f larger than this value. In order to discuss the results in Figs 10 and 11, the stress–strain behavior for various V_f is discussed in association with the failure mechanism. In short fiber composites, the knee point corresponds to the onset of plastic deformation in matrix and damage such as fiber/matrix interfacial debonding and cracking in resin [16]. For low V_f, the knee point means the onset of plastic deformation of resin, and final failure occurs at relatively large strain with little fiber/matrix debonding. In this case, τ_u is related to the interfacial shear strength (τ^* in Fig. 10), which shows a higher value. On the other hand, for higher V_f, the knee point indicates the onset of fiber/matrix debonding because the knee point stress is independent of V_f. After the knee point, debonding takes place progressively and final failure occurs at relatively small strain after large magnitude of debonding. In this case, τ_u is related to the interfacial shear stress due to friction between fiber and resin (τ_d in Fig. 10), which is lower than the strength.

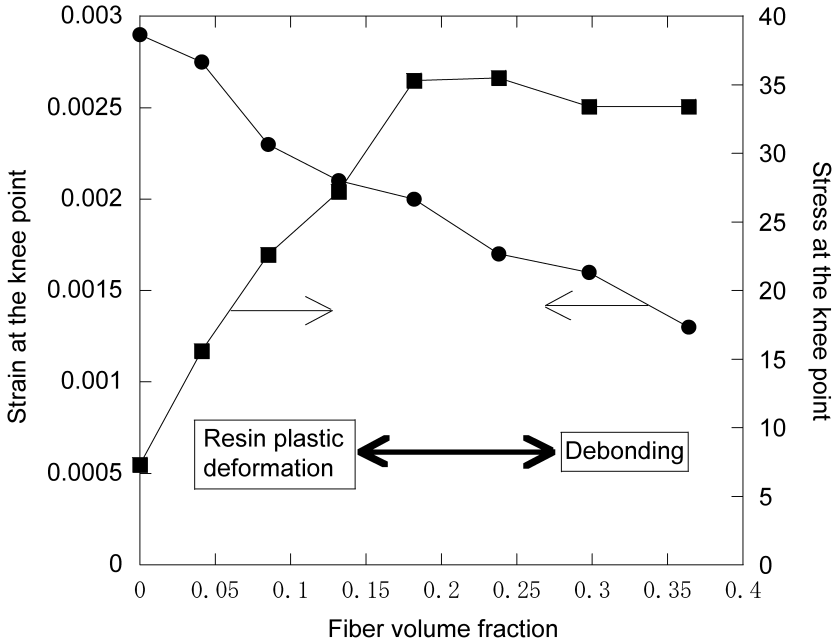

Figure 11. Stress (■) and strain (•) at the knee point in the stress–strain curves.

4. CONCLUSION

Mechanical properties of composites consisting of ABS resin mixed with CFRP pieces are experimentally characterized. The strength and modulus are improved with an increase in CFRP content although strength saturates at CFRP content of 50 wt%. Carbon fibers are not coated by epoxy resin and dispersed individually in ABS resin whilst some fiber bundles coming from the original CFRP pieces are included. The modulus and strength are expressed by simple equations based on the macromechanical model for short fiber composites.

Acknowledgement

This research is supported by a Grant-in-Aid for Cooperation of Innovative Technology and Advanced Research in Evolutional Area (CITY AREA), 2004, from the Ministry of Education, Culture, Sports, Science and Technology of Japan.

REFERENCES

1. Research Report on Systematic Recycling Technology of Wasted FRPs of Large Scale by Government Industrial Research Institutes (1993) (in Japanese).
2. K. Ogi, T. Shinoda and M. Mizui, Strength in concrete reinforced with recycled CFRP pieces, *Composites Part A* **36**, 893–902 (2005).
3. T. Nishikawa, K. Ogi, T. Tanaka, Y. Okano and I. Taketa, Electrical properties of ABS resin reinforced with recycled CFRP, *Adv. Compos. Mater.* **16**, 1–10 (2007).

4. H. L. Cox, The elasticity and strength of paper and other fibrous materials, *Brit. J. Appl. Phys*. **3**, 72–79 (1952).
5. A. Kelly and W. R. Tyson, Tensile properties of fibre-reinforced metals, *J. Mech. Phys. Solid* **13**, 329–350 (1965).
6. P.-A. Eriksson, A.-C. Albertsson, P. Boydell, G. Prautzsch and J.-A. E. Manson, Prediction of mechanical properties of recycled fiberglass reinforced polyamide 66, *Polym. Compos.* **17**, 830–839 (1996).
7. S.-Y. Fu and B. Lauke, Effects of fiber length and fiber orientation distribution on the tensile strength of short-fiber-reinforced polymers, *Compos. Sci. Technol.* **56**, 1179–1190 (1996).
8. Y. T. Zhu, W. R. Blumenthal and T. C. Lowe, The tensile strength of short fiber-reinforced composites, *J. Mater. Sci*. **32**, 2037–2043 (1997).
9. J. W. J. Van Hattum and C. A. Bernardo, A model to predict the strength of short fiber composites, *Polym. Compos.* **20**, 524–533 (1999).
10. S.-Y. Fu, C.-Y. Yue, X. Hu and Y.-W. Mai, Analysis of the micromechanics of stress transfer in single- and multi-fiber pull-out tests, *Compos. Sci. Technol.* **60**, 569–579 (2000).
11. C.-C. Jeng and M. Chen, Flexural failure mechanisms in injection-moulded carbon fibre/PEEK composites, *Compos. Sci. Technol.* **60**, 1863–1872 (2000).
12. S.-Y. Fu, B. Lauke, E. Mader, C.-Y. Yue, X. Hu and Y.-W. Mai, Hybrid effects on tensile properties of hybrid short-glass-fiber and short-carbon-fiber-reinforced polypropylene composites, *J. Mater. Sci.* **36**, 1243–1251 (2001).
13. S.-Y. Fu, B. Lauke, E. Mader, C.-Y. Yue and X. Hu, Tensile properties of short-glass-fiber and short-carbon-fiber-reinforced polypropylene composites, *Composites Part A* **31**, 1117–1125 (2000).
14. J. L. Thomason, Micromechanical parameters from macromechanical measurement on glass-reinforced polybutyleneterepthalate, *Composites Part A* **33**, 331–339 (2002).
15. J. L. Thomason, The influence of fiber length and concentration on the properties of glass fibre reinforced polypropylene: 5 injection moulded long and short fibre PP, *Composites Part A* **33**, 1641–1652 (2002).
16. D. Hull, *An Introduction to Composite Materials*, p. 210. Cambridge University Press, Cambridge, UK (1981).